

Spontaneous Lipid Binding to the Nicotinic Acetylcholine Receptor in a Native Membrane

Liam Sharp¹ and Grace Brannigan^{1,2}

¹*Center for Computational and Integrative Biology, Rutgers University-Camden, Camden, NJ*

²*Department of Physics, Rutgers University-Camden, Camden, NJ*

The nicotinic acetylcholine receptor (nAChR) and other pentameric ligand-gated ion channels (pLGICs) are native to neuronal membranes with an unusual lipid composition. While it is well-established that these receptors can be significantly modulated by lipids, the underlying mechanisms have been primarily studied in model membranes with only a few lipid species. Here we use coarse-grained molecular dynamics (MD) simulation to probe specific binding of lipids in a complex quasi-neuronal membrane. We ran a total of 50 microseconds of simulations of a single nAChR in a membrane composed of 36 species of lipids. Competition between multiple lipid species produces a complex distribution. We find that overall, cholesterol selects for concave intersubunit sites and PUFAs select for convex M4 sites, while monounsaturated and saturated lipids are unenriched in the nAChR boundary. In order to characterize binding to specific sites, we present a novel approach for calculating a “density-threshold affinity” from continuous density distributions. We find that affinity for M4 weakens with chain rigidity, which suggests flexible chains may help relax packing defects caused by the conical protein shape. For any site, PE headgroups have the strongest affinity of all phospholipid headgroups, but anionic lipids still yield moderately high affinities for the M4 sites as expected. We observe cooperative effects between anionic headgroups and saturated chains at the M4 site in the inner leaflet. We also analyze affinities for individual anionic headgroups. Combined, these insights may reconcile several apparently contradictory experiments on the role of anionic phospholipids in modulating nAChR.

I. INTRODUCTION

The nicotinic acetylcholine receptor (nAChR) is a well studied excitatory pentameric ligand gated ion channel (pLGICs). nAChRs are found at high density in post-synaptic membranes and the neuromuscular junction in mammals, and the electric organ in *Torpedo* electric rays. The nAChR is activated by the binding of agonists such as nicotine or acetylcholine to the orthosteric site in the extra-cellular domain (ECD). When post-synaptic nAChRs are activated *en-mass* they stimulate an action potential. Thus nAChRs play a critical role in both cognition and memory¹ and neuromuscular function^{2,3}. nAChR and the greater pLGIC superfamily play various roles in neurological diseases related to inflammation⁴⁻⁷, addiction⁸, chronic pain⁹, Alzheimer's Disease^{3,10-12}, spinal muscular atrophy¹³, schizophrenia^{3,14} and neurological autoimmune diseases^{15,16}.

nAChRs are highly sensitive to their local lipid environment. nAChR poorly conducts ions in model phosphatidylcholine (PC)-only membranes, but can conduct a current with the addition of cholesterol or anionic lipids¹⁷⁻²⁵, though too much cholesterol can also cause a loss of function^{20,26-28}. Functional studies using *Xenopus* oocytes²⁹⁻³⁶ require lipid additives such as asolectin^{20,29-31,33-36} or lipids from synaptic membranes³⁷ to recover native levels of nAChR ion flux. Understanding the mechanism of modulation requires understanding how and where the modulating lipid interacts with the receptor, and these interactions may themselves be dependent upon the rest of the lipid composition.

Mammalian neuronal membranes³⁸⁻⁴¹ have unique compositions compared to other mammalian membranes⁴²⁻⁴⁶. Neuronal membranes are more similar to the membrane of the *Torpedo* electric ray's electric organ^{47,48} than the average mammalian membrane⁴⁶. The neuronal membrane³⁸⁻⁴¹ is rich in lipids in which one or both chains are polyunsaturated fatty acids (PUFAs), particularly the $n - 6$ PUFA arachidonic acid (AA), and the $n - 3$ PUFAs docosahexaenoic acid (DHA) and eicosapentaenoic acid (EPA). These three PUFA's comprise $\sim 20 - 25\%$ of the acyl chains of neuronal phospholipids, and are involved in secondary signaling^{49,50} and neuronal development⁵¹. PUFAs are linked to a number of neurological diseases and disorders that overlap nAChR related diseases. PUFAs play a roll in major depressive and bipolar disorder^{50,52-55}, schizophrenia^{51,53,55-58}, and Alzheimer's Disease^{52,59-63}.

Functional experiments have focused on the role of anionic lipids and cholesterol as modulators of pLGICs^{18-25,64} (the role of polyunsaturation has received comparatively little attention due

to common challenges with oxidation of polyunsaturated chains). Such experiments have been overwhelmingly consistent with a role for direct binding of lipids as a modulatory mechanism. As for most membrane proteins, it is experimentally challenging to capture the boundary lipid composition of pLGIC because lipids are small molecules that may remain partly fluid even in their bound state. Numerous structures of pLGICs have revealed a conserved arrangement for both the TMD and the ECD. In the TMD, each subunit has four membrane helices (M1-M4) with the five subunits forming a “star” shape around a central pore (Figure 1A). The M2 helix lines the pore, the M1 and M3 helices form a middle ring that includes the intersubunit cavities, and the M4 helices form the tip of the star. Structural methods have resolved potential cholesterol molecules^{65,66} and phospholipids⁶⁷⁻⁶⁹ bound to subunit interfaces, but crystallographic disorder introduced by lipids typically precludes identification of lipid species. Mass spectrometry has revealed specific binding of anionic lipids, with additional mutagenesis studies suggesting localized sites in the inner leaflet near the M4 helices.⁷⁰

Molecular dynamics (MD) simulations are particularly useful for visualizing and characterizing microscopic interactions within a fluid system. Given a putative cholesterol or lipid binding mode, atomistic simulations can be used to probe stability of the lipid binding mode. For pentameric channels, such approaches have primarily demonstrated stability of bound cholesterol⁷¹, particularly at intersubunit sites^{65,72}. Unfortunately, fully atomistic simulations suffer from slow diffusion of lipids within the membrane, which prevents spontaneous lipid sorting by proteins over accessible simulation time scales.

Coarse-grained MD simulations use simplified molecular models that can reveal spontaneous lipid sorting, domain formation, and protein partitioning over simulation timescales⁷³⁻⁷⁶. Coarse-grained MD simulations have been used previously to probe interactions of pLGICs with propofol⁷⁷ as well as spontaneous lipid binding in model membranes^{70,78,79}. In previous work, we found that nAChR embedded in multiple domain-forming model membranes partitioned to the PUFA-rich liquid disordered domain⁷⁸, rather than to the cholesterol-rich liquid-ordered or “raft” domain that was suggested by cholesterol modulation. We observed that cholesterol still occupies embedded sites on the nAChR TMD, where it is shielded from the liquid disordered domain. However, native membranes are primarily composed of heteroacidic lipids with two distinct chains, where each chain has a different domain preference; such lipids will naturally destabilize domains. In non-domain forming model membranes composed of heteroacidic lipids, two classes of five-fold symmetric sites emerged: an intersubunit site and the M4 site (Figure

1B). Cholesterol and saturated chains were enriched at the inter-subunit interfaces and n-3 PUFA acyl-chains were enriched around the M4 helices⁷⁹. These results were consistent with binding to minimize packing defects: the rigid lipids could fill in the concave regions at the intersubunit sites while the flexible chains would easily deform around the “star points” of the M4 helices. Yet it was not clear whether these same patterns would be upheld in the more complex environment of a native neuronal membrane, which has many more options for minimizing any packing defect.

Neuronal membranes also contain a sizeable fraction of anionic lipids in the inner leaflet^{38–40}. With collaborators in the Cheng lab, we recently⁷⁰ showed that anionic headgroups bind preferentially to the pLGIC *Erwinia* ligand-gated ion channel (ELIC), when the same acyl chains are used for both headgroups. Through coarse-grained MD, we found specific binding sites for 1-palmitoyl-2-oleoyl phosphatidylglycerol POPG in the intersubunit sites (inner leaflet); these sites contained basic amino acids that were also implicated through mutagenesis⁷⁰. In nAChR the high-density of basic amino acids are in the M4 site (inner leaflet) rather than the intersubunit site (inner leaflet), so we would expect a shift for nAChR even in model membranes, due purely to the protein sequence. The relative roles of headgroup charge vs acyl chain saturation in driving affinity are unknown.

The use of complex quasi-realistic membranes in coarse-grained MD simulations is growing more feasible. In 2014, Ingólfsson et al⁴⁶ simulated an “average mammalian” membrane containing 63 lipids species, followed in 2017 by a coarse-grained neuronal membrane⁴¹. Multiple accessible and realistic membranes have been developed for comparison of protein-lipid interactions between model and quasi-native membranes^{75,76,80–82}. To our knowledge, no such coarse-grained MD simulations using quasi-native membranes have been used with pLGICs.

While the model membranes we used previously are useful for identifying putative sites, they have critical limitations. As stated previously, model membranes typically vary headgroup charge or acyl chain saturation, not both. Model membranes also do not allow for identification of more specific chemical variations within general saturation classes (i.e. n-3 PUFAs like DHA vs n-6 PUFAs like α -linolenic acid) or like-charged head groups (PC vs PE, or phosphoserine (PS) vs phosphoinositol (PI)). For this work, we embed the neuromuscular nAChR⁸³ in a coarse-grained neuronal membrane⁴¹. To test whether the predictions we developed from model membranes hold for native membranes, we develop a new method for quantifying affinities for partially-occupied binding sites.

The remainder of this paper is organized as follows. Section II presents our simulation and

analysis approach, including introduction of the density-threshold affinity. Section III presents results and discussion of site selectivity of neutral lipids, followed by a reoriented discussion of the same data that is focused on lipid preferences of individual sites. We then consider selectivity of anionic lipids in the inner leaflet and finally consider the effects of specific headgroup differences. Section IV concludes.

II. METHODS

A. Simulation Composition

All simulations used the coarse-grained MARTINI 2.2⁸⁴ topology and forcefield. nAChR coordinates were based on a cryo-EM structure of the $\alpha\beta\gamma\delta$ muscle-type receptor in native torpedo membrane (PDB 2BG9⁸³). This is a medium resolution structure (4Å) and was further coarse-grained using the martinize.py script; medium resolution is sufficient for use in coarse-grained simulation, and the native lipid environment of the proteins used to construct 2BG9 is critical for the present study. The secondary, tertiary and quaternary structure in 2BG9 was preserved via soft backbone restraints during simulation as described below, so any inaccuracies in local residue-residue interactions would not cause instability in the global conformation.

nAChR was embedded in a coarse-grained neuronal membrane based on Ingólfsson et al⁴¹. The neuronal membrane from described by Ingólfsson contains phospholipids, sterols, diacylglycerol, and ceramide. Membranes presented in this paper only consider phospholipids and cholesterol, for a total of 36 unique lipid species, see Table SI 1.

Coarse-grained membranes were built using the MARTINI script insane.py⁸⁵, which was also used to embed the coarse-grained nAChR within the membrane. The insane.py script randomly places lipids throughout the inter- and extra-cellular leaflets, and each simulation presented in this manuscript was built separately. All simulation box sizes were 40x40x35 nm³ with $\sim 4,500 - 5,000$ lipids and total $\sim 450,000$ beads.

B. Simulations

Molecular dynamics simulations run using the MARTINI 2.2⁸⁴ forcefield and GROMACS^{86,87} 2019.2. All systems used van der Waals (vdW) and Electrostatics with reaction-field and a dielectric constant of $\epsilon_r=15$ and electrostatic cutoff length at 1.1 nm. Energy minimization was

performed for 1000000 steps, but energy minimization tended to concluded after $\sim 5000 - 10000$ steps.

Volume and pressure equilibrations were run with isothermal-isochoric (NVT) and isothermal-isobaric (NPT) ensembles respectively. NVT and NPT simulations used a time step of 15 fs and run for 0.3 ns using Berendsen thermostat held at a temperature of 323 K, and Berendsen pressure coupling with compressibility set to $3 \times 10^{-5} \text{ bar}^{-1}$ and a pressure coupling constant set to 3.0 ps for the NPT ensemble.

Molecular dynamics simulations were run using a time step of 20 fs for 5 μs for 10 replicas. Simulations were conducted in the NPT ensemble, by using the velocity rescaling to a temperature of 323 K with a coupling constant set to 1 ps. Semi-isotropic pressure coupling was set to Parrinello-Rahman with compressibility at $3 \times 10^{-5} \text{ bar}^{-1}$ and pressure coupling constant set to 3.0 ps.

Secondary structures restraints with MARTINI recommendations were constructed by the martinize.py⁸⁴ script and imposed by GROMACS^{86,87}. The nAChR conformation was preserved by harmonic bonds between backbone beads separated by less than 0.5 nm and calculated using the ElnDyn algorithm⁸⁸ associated with MARTINI⁸⁴ with a coefficient of $900 \text{ kJ}\cdot\text{mol}^{-1}$.

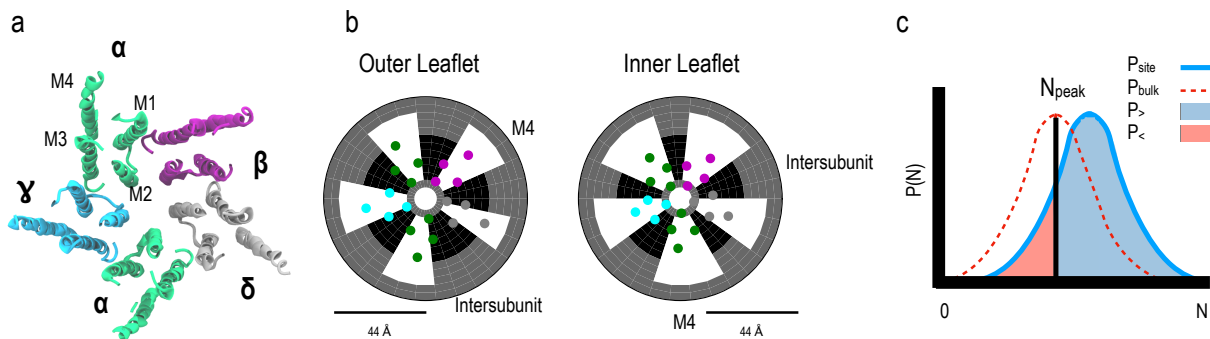


FIG. 1. Binding site boundaries and distribution definitions. (a) Structure of the nAChRTMD⁸³, viewed from the extracellular domain. Helices are colored by subunit (α :green, β :purple, γ : cyan, δ :grey). (b) Boundaries of the pseudo-symmetric intersubunit (black) and M4 (white) sites. The angular components are determined by the location of the M1 and M3 alpha-helices for either two adjacent subunits (intersubunit sites) or a single subunit (M4 sites), and are listed in Table S5. Circles correspond to the helices shown in panel A. (c) The distributions $P_{site}(n)$ (blue) and $P_{bulk}(n)$ (dashed red) represent the probability distributions for number of beads of a certain lipid species in the site or in an analogously-sized area of the bulk, respectively. The value n_{peak} maximizes P_{bulk} . $P_{<}$ (pink) is the area under P_{site} to the right of n_{peak} while $P_{>}$ (light blue) is the area under P_{site} to the right of n_{peak} .

C. Calculation of Polar Density Distributions

As in our previous work^{70,78,79}, the two-dimensional density distribution ρ_B of the beads within a given lipid species B around the protein was calculated on a polar grid:

$$\rho_B(r_i, \theta_j) = \frac{\langle n_B(r_i, \theta_j) \rangle}{r_i \Delta r \Delta \theta} \quad (1)$$

where $r_i = i\Delta r$ is the projected distance of the bin center from the protein center, $\theta_j = j\Delta\theta$ is the polar angle associated with bin j , $\Delta r = 10\text{\AA}$ and $\Delta\theta = \frac{\pi}{15}$ radians are the bin widths in the radial and angular direction respectively, and $\langle n_B(r_i, \theta_j) \rangle$ is the time-averaged number of beads of lipid species B found within the bin centered around radius r_i and polar angle θ_j . In order to determine enrichment or depletion, the normalized density $\tilde{\rho}_B(r_i, \theta_j)$ is calculated by dividing by the approximate expected density of beads of lipid type B in a random mixture, $x_{BSB} N_L / \langle L^2 \rangle$, where s_B is the number of beads in one lipid of species B , N_L is the total number of lipids in the system, and $\langle L^2 \rangle$ is the average projected box area:

$$\tilde{\rho}_B(r_i, \theta_j) = \frac{\rho_B(r_i, \theta_j)}{x_{BSB} N_L / \langle L^2 \rangle} \quad (2)$$

where the expected density is derived at the first frame of the simulation. Python software for these calculations are under active development and are located at⁸⁹.

This expression is approximate because it does not correct for the protein footprint or any undulation-induced deviations of the membrane area. The associated corrections are small compared to the membrane area and would shift the expected density for all species equally, without affecting the comparisons we perform here. For a given lipid species or class, analysis excluded any replicas in which fewer than 5 lipids of the species/class were in the leaflet at any point in the sampled simulation.

D. Calculation of the density-threshold affinity

Although lipids to occupy clearly detectable hot-spots, binding to these sites are not straightforward to describe by a traditional two-state model. Lipids are chains that may partially occupy or fully occupy a site, and they may share a site with another lipid that is partly or fully occupying the site. While the standard affinity can be determined from the probability of single occupancy,

the density-threshold affinity is determined from the probability that a site is occupied by more beads than would be expected based on bulk density.

For a given site, consider two probability distributions: the probability $P_{site}(n)$ of finding n beads within the site and the probability $P_{bulk}(n)$ of finding n beads within a region of equivalent area in the bulk, respectively. For a lipid that has no affinity for this binding site, we expect $P_{site}(n) = P_{bulk}(n)$, while $P_{site}(n)$ should be right-shifted for a strong affinity and left-shifted in the presence of competition. We calculate the degree of right or left shift by first finding the number of beads n_{peak} that corresponds to the peak of the density distribution in the bulk. As illustrated in Figure 1 C, we then integrate P_{site} on both the left and right side of the threshold n_{peak} to yield $P_{<}$ and $P_{>}$ respectively:

$$P_{<} \equiv \sum_{n \leq n_{peak}} P_{site}(n) \quad (3)$$

$$P_{>} \equiv \sum_{n > n_{peak}} P_{site}(n) \quad (4)$$

Note that this step breaks the distribution into two macrostates on either side of the threshold, allowing clear analogy with a classic binary binding model. The free energy difference between the two macrostates is

$$\Delta G = -RT \ln \frac{P_{>}}{P_{<}} \quad (5)$$

where R is the gas constant and T is temperature. We term this free energy difference the “density-threshold affinity”. In the special case of binary occupancy,

$$P_{site}(n) = \begin{cases} (1 + K_D/[L])^{-1}, & \text{if } n = 1 \\ (1 + [L]/K_D)^{-1}, & n = 0 \end{cases} \quad (6)$$

where K_D is the dissociation constant and $[L]$ is the ligand concentration. In a dilute solution the volume per ligand is typically much larger than the site volume, so $P_{bulk}(n) = 1$ for $n = 0$ and vanishes for all $n > 0$, so $n_{peak} = 0$. Consequently, for this special case, $P_{<} = (1 + [L]/K_D)^{-1}$ and $P_{>} = (1 + K_D/[L])^{-1}$. Then Equation 5 reduces to the classic form for the chemical potential $RT \ln K_D - RT \ln [L]$.

E. Binding Site Definition and Occupancy Calculations

We consider two classes of site: intersubunit sites and M4 sites. Each pLGIC has ten of each site (five in the outer leaflet and five in the lower leaflet) for a total of twenty sites (Figure 1B). The boundaries for each site were drawn to correspond to the localized binding hot spots observed for heteroacidic membranes⁷⁹, and are non-overlapping. Inter-subunit sites include bins with angular components between the M1 and M3 alpha-helices of two adjacent subunits, and a radial component satisfying $10 < r \leq 32\text{\AA}$. M4 sites include bins with complementary angular components (so that no sites overlap) falling within the M1 and M3 alpha-helices of a single subunit, and a radial component satisfying $10 < r \leq 44\text{\AA}$. For a full description of radial and angular dependencies, please see Table SI 4.

In order to calculate $P_{site}(n)$, a distribution was taken across frames at 10 ns intervals. For any frame, the beads of a given lipid or chain type were binned onto a fine polar grid with $\Delta r = 4\text{\AA}$ and $\Delta\theta = \frac{\pi}{25}$. The bins falling within the site boundaries were then summed to calculate the occupancy n . This approach allowed for straightforward adjustment of site boundaries if needed without needing to re-bin the whole trajectory.

F. Calculation of Accessible Area

Calculation of P_{bulk} requires determining the accessible site area in order to calculate the densities in a bulk region of similar area. The area A accessible to the lipids is the difference between the total site area A_{tot} and the area A_{ex} excluded by the protein: $A = A_{tot} - A_{ex}$. A_{tot} is straightforward to calculate by summing over the areas of the bins i within the site boundaries: $A_{tot} = \sum_i r_i \Delta r_i \Delta\theta_i$. Calculating A_{ex} is less straightforward, and although there are many possible ways to do this, for self-consistency we used the same tools from our primary analysis.

In a single lipid membrane, $P_{site}(n) = P_{bulk}(n)$ as long as $P_{bulk}(n)$ is calculated using the proper area A . We exploit this identity to calculate A for each site, by running a single nAChR in pure di-palmitoyl phosphatidylcholine (DPPC) for ~ 370 ns and determining the value of A for each site such that $P_{site}(n)$ and $P_{bulk}(n)$ have the same peak. These areas are reported in Table SI 4.

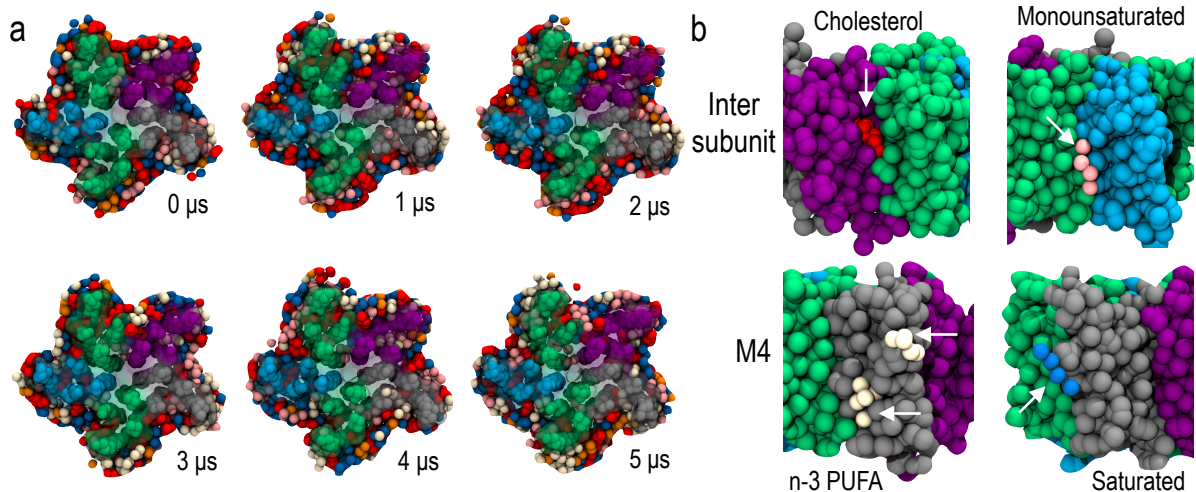


FIG. 2. A molecular perspective of coarse-grained simulation results. a) Multiple frames from a single simulation replica over 5 μs . The nAChR TMD is shown in surface representation and colored as in Figure 1. Cholesterol and acyl chains within 15 Å of nAChR are shown as beads, and colored by chain type: saturated lipids: blue, monounsaturated lipids: orange, n-6 PUFAs: pink, n-3 PUFAs: beige, and cholesterol: red. Each phospholipid color includes several lipid species of the same type, and simulations included a larger membrane and the ECD, which is not shown. b) Representative poses of lipids for individual sites, colored as in A, but viewed from within the membrane looking at the TMD surface. Cholesterol selects for the intersubunit site while monounsaturated lipids have a particularly low affinity for this site. PUFAs select for the M4 site, while saturated lipids have a particularly low affinity.

III. RESULTS AND DISCUSSION

A. Effect of acyl chain on site selectivity among neutral lipids

Representative frames from a typical trajectory of boundary lipids are shown in Figure 2A, with representative poses shown in Figure 2B. In order to quantitatively compare the lipid distributions for the native system to our previous model system, we plotted the enrichment of boundary density relative to bulk density on a two-dimensional polar heat map centered around the protein. This enrichment is shown in Figure 3A for cholesterol and various acyl chains grouped by saturation. Saturated and monounsaturated acyl chains are not significantly depleted or enriched in the boundary of the protein. Regions of cholesterol density are much more localized than in the model membrane (Figure 3C), with pockets of high enrichment very close to the protein and weak depletion in the remainder of the boundary region. Both n-6 and n-3 PUFA chains yield five-fold symmetric enrichment around the M4 alpha-helices, as observed for n-3 PUFAs in the model membrane. In the neuronal membrane, however, this enrichment is less well-defined and

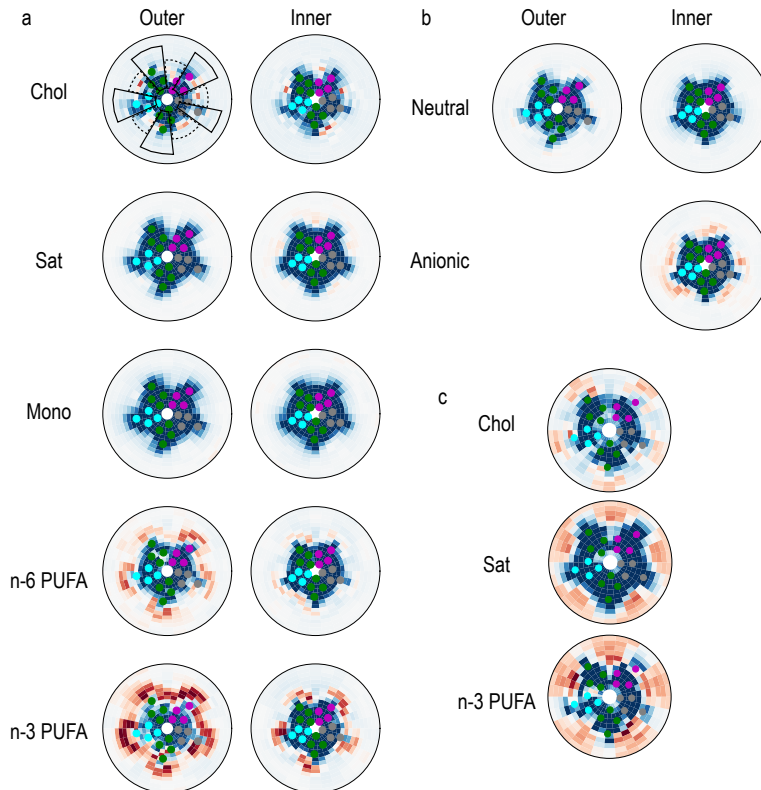


FIG. 3. Lipid density enrichment around a central singular nAChR. (a) and (b) Density enrichment $\tilde{\rho}_a$ for lipids in a neuronal membrane, calculated using eq 2 for both outer and inner leaflets, averaged over 10 replicas for $2.5 \mu\text{s}$ each. The maximum radius from the nAChR pore is 60 \AA . Depletion relative to a random mixture ($\log \tilde{\rho}_a < 0$) is blue while enrichment ($\log \tilde{\rho}_a > 0$) is red. Lipids are organized by acyl chain (a) or headgroup (b). Acyl chain density includes only the relevant chain of a heteroacidic lipid, while headgroup density includes the whole lipid. Helices are represented as circles colored as in Figure 1. Intersubunit (solid line) and M4 (dashed line) site boundaries are marked. (c) Equivalent analysis for nAChR in a model membrane of 2:2:1 n-3 PUFA:saturated:cholesterol, using previously published trajectories⁷⁹.

spreads into the intersubunit regions. In particular, additional pockets of significant enrichment are apparent in the $\beta - \delta$ subunit interface in the outer leaflet. The overall area of the regions of PUFA-enrichment decrease in the inner leaflet, where n-3 PUFAs are enriched around M4 helices, but n-6 PUFA density is not five-fold symmetric and has weak enrichment. Overall, the loss of definition in site boundaries diverges from the well-defined five fold enrichment for n-3 PUFAs we saw in model membranes⁷⁹.

In order to reduce these distributions to affinities that are more straightforward to interpret, we calculated the density-threshold affinity ΔG for various lipid species as defined in Eq. 5. We organize this information in two different ways: Figure 4 provides the “lipid’s perspective” and is organized to identify the preferred site for a given lipid type (the lipids’ “site selectivity”), while

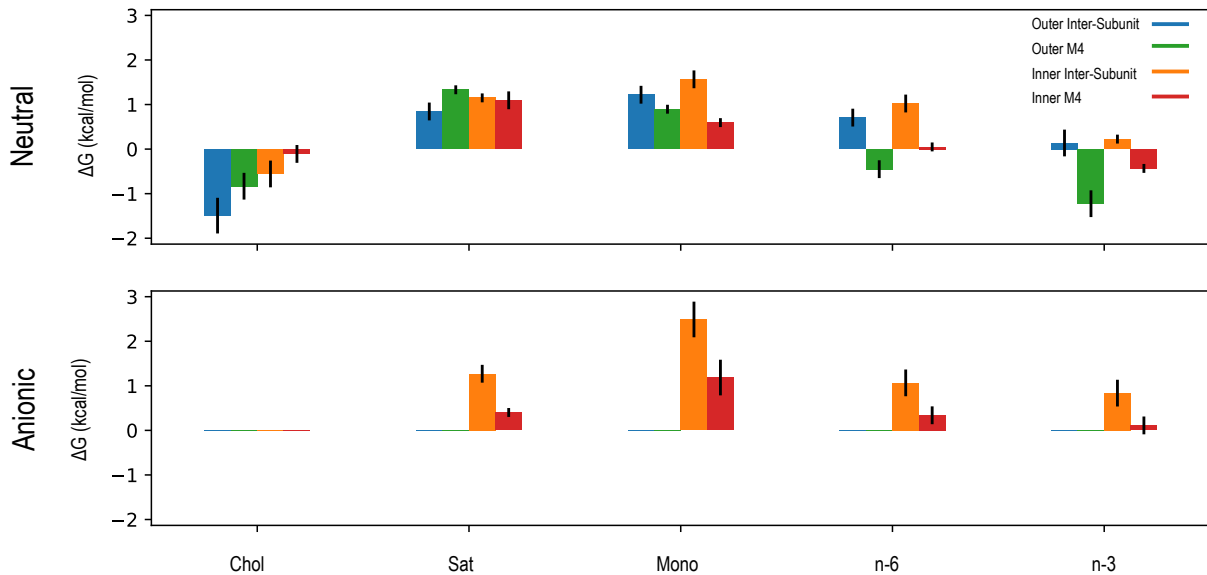


FIG. 4. Density-threshold affinities organized to reveal site selectivity. The density-threshold affinities (ΔG) are calculated using Equation 5, where error bars are the standard error ($n=10$ independent replicas). Density-threshold affinities are colored by site; in the outer leaflet: intersubunit (blue) and M4 (green), and for the inner leaflet: intersubunit (orange) and M4 (red). Values are separated by headgroup charge (rows) and acyl chain type (columns). More negative values indicate stronger affinities, while more positive values indicate more displacement of the lipid by other lipid species. Data incorporates 10 replicas averaging over the last half of the $5\mu s$ trajectory, with five-fold averaging over each type of pseudosymmetric site. Figure 5 has an alternate representation of the same data.

Figure 5 provides the “site’s perspective” and is organized to identify the most favorable lipids for a given site (the sites’ “lipid specificity”).

We first consider site selectivity for neutral lipids. Affinities for neutral lipids and cholesterol are shown in Figure 4A, where more negative values of ΔG indicate a stronger density-threshold affinity and more positive values indicate more displacement by other lipids. Overall, as shown in Figure 4A, saturated lipids have similar density-threshold affinities across all sites, which is consistent with the generally flat distribution observed in Figure 3. Yet saturated lipids do yield a slightly stronger affinity for intersubunit sites, at least in the outer leaflet, which may drive the high amount of saturated enrichment observed at these sites in model membranes. Outer leaflet monounsaturated lipids are slightly more unfavorable in intersubunit sites than M4 sites, and this difference grows in the inner leaflet.

In contrast to saturated and monounsaturated lipids, PUFAs and cholesterol are highly selective for particular sites. As shown in Figure 4A, neutral PUFAs have significantly stronger affinities for

M4 sites than for innersubunit sites in the same leaflet. Such selectivity is consistent with the PUFA enrichment density in Figure 3A, where n-3 PUFAs can occupy most regions of the TMD but have particularly high levels of enrichment around M4. It is further consistent with our expectations from model membranes (Figure 3C). Regardless of the site class, PUFAs favor the outer leaflet site over the inner leaflet site, but both sets of M4 sites are more favorable than both sets of intersubunit sites. Conversely, cholesterol has significantly stronger affinities for innersubunit sites than for M4 sites, which is also consistent with the enrichment density in Figure 3A and our expectations from model membranes (Figure 3C). For cholesterol, however, the leaflet is a bigger determinant of affinity than the site; cholesterol has a stronger affinity for either outer leaflet site compared to either inner leaflet site.

B. Lipid preferences of intersubunit and M4 sites

We now switch perspectives to considering which neutral lipids are most favorable for particular sites. As shown in Figure 5 A and B, intersubunit sites in both leaflets prefer cholesterol to phospholipids, which is expected based on the results from model membranes. Upon visual inspection, this result may appear to diverge from the cholesterol polar density plots in neuronal membranes (Figure 3 A). The present results show that while the overall footprint of cholesterol enrichment in (Figure 3 A) is small, this small region actually reflects a tight and persistently occupied binding site. The highly right-shifted distributions for cholesterol are shown in Figure S1.

PUFA chains yield affinities for the intersubunit site that are approximately >0.5 kcal/mol stronger than saturated lipid affinities (Figure 5 A and B), which was unexpected based on results from model membranes but is consistent with the corresponding enrichment density in Figure 3A. More generally, neutral phospholipid affinities for intersubunit sites obey the following trend, from strongest to weakest: n-3 $>$ n-6 $>$ saturated $>$ monounsaturated. Thus, even though PUFA chains prefer M4 sites to intersubunit sites, and saturated chains prefer intersubunit sites to M4 sites, PUFAs have a stronger affinity for either site type than do saturated lipids.

For intersubunit sites, monounsaturated lipids have the weakest affinities (> 0.5 kcal/mol), which may reflect a limited number of ways to pack the single kink of a monounsaturated chain in this concave site. In contrast, cholesterol and PUFAs are either small or highly flexible and may more easily pack across multiple sites. Saturated chains may pack parallel to the protein surface

in these sites.

As shown in Figure 5C and D, M4 sites in both leaflets have the strongest affinity for n-3 PUFAs, and affinity weakens as acyl chain rigidity increases; from strongest to weakest the phospholipid affinities follow: n-3 > n-6 > monounsaturated > saturated. This is consistent with a role for PUFAs in minimizing unfavorable membrane deformations caused by the pLGIC's conical-star shape.^{90–95} Surprisingly, cholesterol had a stronger affinity for M4 sites than any acyl chains other than n-3 PUFAs. Cholesterol is rigid, small, and has asymmetric sides (rough and smooth) which potentially allows it to embed between alpha-helices and compete with n-3 PUFAs for binding. Any cholesterol bound within the grooves of the subunit interface (as hypothesized based on atomistic simulations⁷¹ and observed in β subunits of nAChR (using coarse-grained simulations⁷⁸), will also get counted within the M4 site.

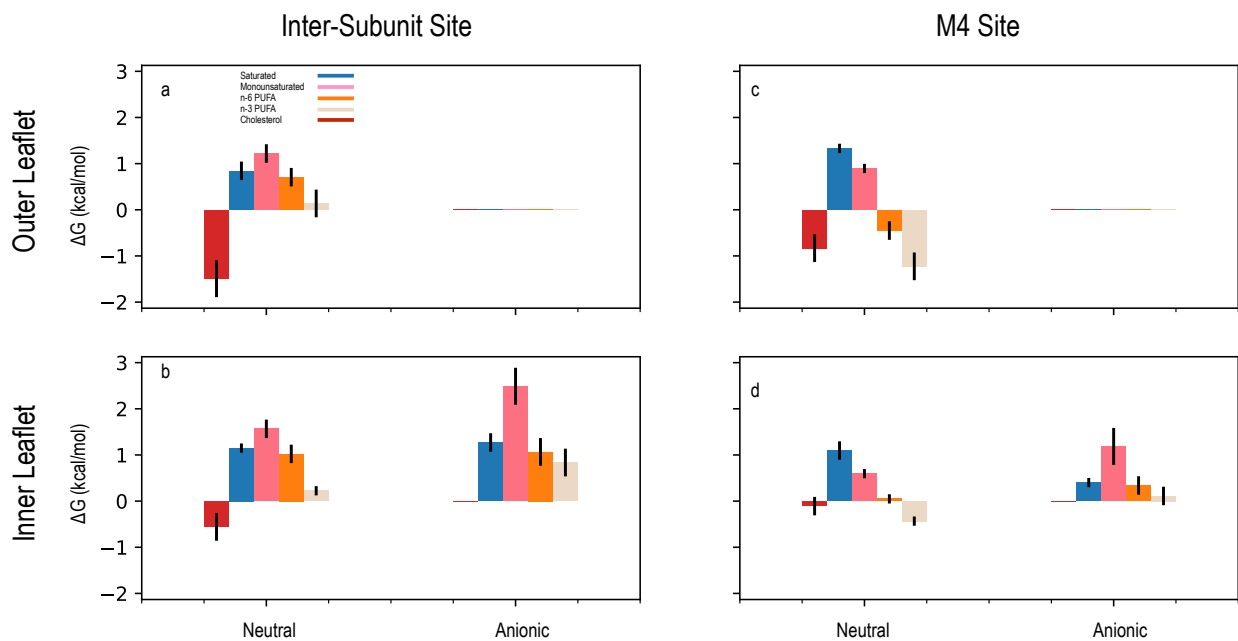


FIG. 5. Density-threshold affinities organized to reveal lipid preferences by site. Data shown is identical but reorganized and recolored from Figure 4. Here, density-threshold affinities are colored by chain type (Saturated:blue, Monounsaturated:pink, n-6 PUFAs:orange, n-3 PUFAs:tan, Cholesterol:red), and separated by leaflet (rows) and site (columns).

C. Effect of Head Group Charge on Affinity Depends on Leaflet and Binding Site

Figure 3b compares the density enrichment for anionic headgroups with that of neutral headgroups. Data is shown for the inner leaflet only, because anionic lipids are not present in the outer leaflet at the start of simulations and few anionic lipids flip flop to the outer leaflet.

In the inner leaflet, the anionic lipids are expected to select for sites that are lined with basic amino acids, which are in different locations depending on subunit (Figure ??) As shown in Figure 3b, anionic lipids are generally enriched around the M3/M4 helices for the α_γ , γ , δ , and β subunits. Anionic lipids are enriched at intersubunit sites and around M4 sites for all subunits but the α subunits. Non- α nAChR subunits have basic amino acids closer to M4 alpha-helices, as shown in Figure SI 2a. We incorporate data from all five pseudo-symmetric sites to obtain the density-threshold affinities reported in Figure 4B, which suggest that anionic lipids have significantly stronger affinities for M4 sites on average. The average anionic affinity difference between intersubunit and M4 sites is ~ -1.0 kcal/mol, as shown in Figures 4, 5d and SI Table 2. Although the magnitude of the affinity difference varies with acyl chain saturation, the sign is unchanged. We now switch again to the “site perspective” to compare whether inner leaflet sites would prefer occupancy by anionic or neutral lipids. As shown in Figure 5C, lipid affinity values for intersubunit sites are either insensitive to charge (saturated or n-6 PUFA chains) or weaker for anionic lipids by at least 0.5 kcal/mol (monounsaturated and n-3 PUFA chains). In comparison, at the M4 site, saturated chains in anionic lipids have significantly stronger affinities than those in neutral lipids (a difference of ~ 0.5 kcal/mol). All other lipid chains attached to anionic headgroups have weaker affinities for the M4 site. The clear trend observed in neutral lipids (stronger affinities for more flexible acyl chains) is thus broken in anionic lipids because saturated anionic lipids are so favorable.

In summary, we observe that binding sites have clear preferences for particular head group charge and acyl-chain saturation, suggesting nAChR lipid occupancy to be driven in two steps, a “coarse-sorting” by head groups, and then “fine-sorting” by acyl-chains. A neutral lipid will occupy nAChR’s boundary region but acyl chains dictate where specific lipids occupy nAChR. Anionic lipids diverge from this pattern at the inner M4 site which has the strongest affinity for anionic lipids independent of saturation.

TABLE I. Density-threshold affinities() of neutral lipids for both sites in the outer leaflet, by head group. Errors are standard errors (n=10 independent replicas).

	Intersubunit Sites ΔG (kcal/mol)	M4 Sites ΔG (kcal/mol)
PE	-0.2 ± 0.3	-1.1 ± 0.2
PC	1.4 ± 0.2	1.1 ± 0.2

D. Role of Individual Lipid Headgroups in Determining Affinity

Neutral and anionic are bulk terms that categorize numerous lipid head-groups by charge. To understand the role of the chemical distinctions between head groups of like charge, we broke the headgroup affinities down by headgroup species in Table I. In the outer leaflet, lipids contain a mixture of PE and PC headgroups. The small neutral PE head group has the strongest affinity across all headgroups for both inter-subunit and M4 sites, -0.2 ± 0.3 and -1.1 ± 0.2 kcal/mol respectively. The larger neutral PC headgroups are weaker than PE by $\sim > 0.5$ kcal/mol. In living cells, as in this neuronal membrane, PUFAs are more frequently tethered to PE than to PC or SM^{38-41,45}, so it is possible that this affinity simply reflects the high affinity of PUFA chains. However, even for identical chains, both experimental and simulation data⁷⁸ suggests stronger PE-ELIC than PC-ELIC interactions.

Table II shows specific head group affinities in the inner leaflet. As in the outer leaflet, lipids with PE headgroups still have the strongest affinity of all lipids, but in the inner leaflet we are also able to distinguish affinities for anionic species. For the intersubunit site, PI, PS, and PC have similar affinities (within statistical error), and have significantly stronger affinities for these sites than the phosphoinositides (PIPS) PIP1, PIP2, PIP3, which have a significantly stronger affinity than phosphatidic acid (PA). Thus, from strongest to weakest, $PE > PI \sim PS \sim PC >> PIP1 \sim PIP2 \sim PIP3 >> PA$ for the intersubunit site. In contrast, at the M4 site, more significant differences among moderate affinity headgroups emerge. PI has significantly stronger affinity than PS (a difference of 0.3 ± 0.1 kcal/mol), and PS has a significantly stronger affinity than PC (a difference of 0.2 ± 0.1 kcal/mol). From strongest to weakest, $PE > PI > PS > PC >> PIP1 \sim PIP2 \sim PIP3 \sim PA$ for the M4 site.

TABLE II. Density-threshold affinities(ΔG) of neutral lipids for both sites in the inner leaflet, by head group. Values are sorted by strength of affinity for intersubunit sites. Errors are standard errors (n=10 independent replicas).

	Inner Inter Sites ΔG (kcal/mol)	Inner M4 Sites ΔG (kcal/mol)
PE	0.3 ± 0.2	-0.1 ± 0.1
PI	0.9 ± 0.3	0.2 ± 0.1
PS	1.0 ± 0.2	0.4 ± 0.1
PC	1.0 ± 0.2	0.9 ± 0.1
PIP3	2.6 ± 0.4	1.8 ± 0.4
PIP2	2.8 ± 0.2	2.1 ± 0.4
PIP1	2.4 ± 0.3	2.1 ± 0.4
PA	3.0 ± 0.3	2.2 ± 0.4

IV. CONCLUSIONS

Using coarse-grained simulations of the nAChR within a quasi-neuronal membrane containing over thirty lipid species, we have observed spontaneous lipid binding and quantified lipid specificity for two types of sites in the protein TMD. These two site classes represent the most concave (intersubunit site) and convex (M4 site) portions of the star-shaped nAChR and were initially observed as “hot spots” in our previous simulations^{70,79} of model membranes. Compared to classic ligand binding sites, these sites are superficial and have a large volume. The “ligands” occupying them are also non-traditional: lipids are flexible chain molecules that may only partially occupy the site and are likely to share the site with other partially-occupying ligands. While our lab has developed promising alchemical approaches⁹⁶ for calculating traditional affinities of atomistic lipids for more highly localized, well-defined sites, these hot spots required a different approach. Here we have proposed a softer “density-threshold affinity” for characterizing these affinities from spontaneous, unbiased coarse-grained simulations. While we restrict the use of this method here to nAChR, it should be straightforward to extend to any other transmembrane proteins with detectable regions of density enrichment.

Our results are summarized graphically in Figure 6. Based on our results from model membranes, we had hypothesized that PUFAs would select for the convex M4 sites and that raft-forming lipids like cholesterol and saturated lipids would select for the concave inter-subunit sites. Overall, our results were consistent with this expectation. Yet although lipids containing PUFAs do prefer the M4 site to the intersubunit site, their affinity for even the intersubunit sites are stronger than that of all other phospholipids. This result underscores the reliable partitioning of

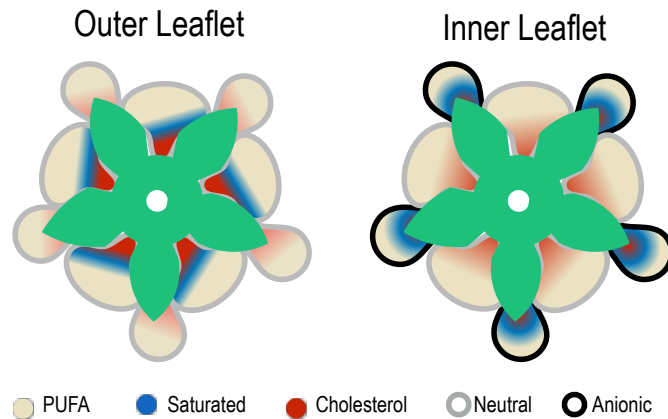


FIG. 6. Cartoon of expected boundary lipids for the nAChR in a native membrane for both leaflets. Protein is shown in the center of both leaflets in a cyan floral shape. Grey and black outlines depict sites favorable for neutral and anionic lipids respectively. Fill color represents the lipids most likely to occupy each site (red: cholesterol, blue: saturated, beige: PUFA) and outline represents headgroup charge (gray: neutral, black: anionic).

nAChR to PUFA-rich, liquid-disordered domains that we observed in homoacidic, domain forming membranes⁷⁸, and suggests PUFAs may have been absent from the intersubunit site in heteroacidic membranes⁷⁹ because of the constraints of the lipid topology. In the latter simulations, all lipids contained one saturated chain and one PUFA chain, so binding of the PUFA chain to its preferred M4 site requires the saturated chain to find the most favorable location nearby (in the intersubunit site) and may block binding of other PUFA chains to that site. These constraints are relaxed in the native neuronal membrane, which has a more diverse lipid composition with multiple different chain pairings; about 6% of the phospholipids in our simulated membranes contain no saturated chain at all. Nonetheless, our previous results⁷⁹ using simplified binary heteroacidic/cholesterol membranes played a key role in identifying the natural site boundaries.

As expected, within each leaflet cholesterol has the strongest affinity for the inter-subunit sites, although the affinity of cholesterol for the M4 sites was second only to that of n-3 PUFAs. Combined, these results are consistent with an overwhelming amount of evidence spanning four decades that suggests direct interactions between cholesterol and nAChRs, regardless of the phospholipid composition of the membrane. One surprise for cholesterol was the role of the leaflet in determining affinity: cholesterol has a stronger affinity for either outer leaflet site compared to either inner leaflet site. This result may reflect competition with anionic saturated lipids in the inner leaflet, which would be consistent with multiple experiments⁹⁷⁻¹⁰⁰, suggesting that anionic lipids can partially or fully compensate for a loss of cholesterol. This result is also consistent with

cholesterol embedded⁷¹ in the outer TMD (which has numerous gaps in the amino acid density) but not the inner TMD.

Based on our results using ELIC⁷⁰, we had expected that anionic lipids would select for sites on the inner leaflet lined with basic residues. In the homomeric ELIC, these residues are symmetrically-arranged, while in the heteromeric nAChR they vary by subunit(Figure ??a), with the M4 site containing the most such residues on most subunits. The present results support that expectation: anionic lipids have a stronger affinity for M4 than inter-subunit sites.

For both outer and inner leaflets, neutral lipids with smaller head groups (PE) have stronger affinity than the larger PC headgroup. It is unclear why PE is more favorable than other neutral lipids at this time, though this is consistent with previous work^{70,78}, and the most straightforward explanation is that the smaller headgroup introduces fewer clashes with the protein TMD.

Among anionic lipids in the inner leaflet, regardless of the site, PS and PI have an affinity greater than or equal to PC, and much greater than the other anionic lipid headgroups (PIP1,PIP2,PIP3, and PA). The lipid headgroups PS and PI both have a charge of -1, while PA in the MARTINI forcefield⁸⁴ carries a charge of -2, and PIP1, PIP2, and PIP3 have charges of -3,-5, and -7. These results suggest that the inner leaflet sites select for monoanionic headgroups, while multianionic headgroups are highly unfavorable. Due to the limitations of the coarse-grained model, future atomistic calculations are required to validate and understand the apparent preference of the M4 site for PI over PS.

The present results highlight the utility of model membranes for developing hypotheses of specific lipid-protein interactions, and the need to test those hypothesis within more complex native membranes. The present results could be tested and aid in interpretation of experiments carried out in more complex membranes. For instance, we would expect that mutations of the basic residues facing the inner leaflet would reduce binding of saturated phospholipids with anionic headgroups, which would be replaced with bound cholesterol. We would also predict that if PUFAs cause gain of function via binding to the intersubunit site, this gain would be enhanced by replacing some heteroacidic lipids with homoacidic lipids while keeping the total fraction of PUFA chains constant. In general the present results provide valuable insight into how to predict lipid competition, which is one of the primarily challenges of interpreting experiments in complex membranes.

ACKNOWLEDGMENTS

GB and LS were supported by the Busch Biomedical Foundation. This project was supported by generous allocation through the Rutgers University Office of Advanced Research Computing (OARC), which is supported by Rutgers University and the state of New Jersey. We are grateful to Dr. Jérôme Hénin for helpful input and suggestions.

DATA AVAILABILITY STATEMENT

The data that support the findings of this study are available from the corresponding author upon reasonable request. Scripts for polar density analysis and plotting scripts can be found on github: <https://github.com/BranniganLab/densitymap>.

REFERENCES

- ¹C. M. Hénault, J. Sun, J. P. D. Therien, C. J. B. DaCosta, C. L. Carswell, J. M. Labriola, P. F. Juranka, J. E. Baenziger, The role of the M4 lipid-sensor in the folding, trafficking, and allosteric modulation of nicotinic acetylcholine receptors, *Neuropharmacology* 96 (2015) 157–168.
- ²N. Mukhtasimova, C. J. B. DaCosta, S. M. Sine, Improved resolution of single channel dwell times reveals mechanisms of binding, priming, and gating in muscle AChR, *The Journal of General Physiology* 148 (2016) 43–63.
- ³D. Kalamida, K. Poulas, V. Avramopoulou, E. Fostieri, G. Lagoumintzis, K. Lazaridis, A. Sideri, M. Zouridakis, S. J. Tzartos, Muscle and neuronal nicotinic acetylcholine receptors: Structure, function and pathogenicity, *FEBS Journal* 274 (2007) 3799–3845.
- ⁴A. Taly, P.-J. Corringer, D. Guedin, P. Lestage, J.-P. Changeux, Nicotinic receptors: allosteric transitions and therapeutic targets in the nervous system, *Nature Reviews Drug Discovery* 8 (2009) 733–750.
- ⁵H. Patel, J. McIntire, S. Ryan, A. Dunah, R. Loring, Anti-inflammatory effects of astroglial $\alpha 7$ nicotinic acetylcholine receptors are mediated by inhibition of the NF- κ B pathway and activation of the Nrf2 pathway., *Journal of neuroinflammation* 14 (2017) 192.
- ⁶G. T. Yocum, D. L. Turner, J. Danielsson, M. B. Barajas, Y. Zhang, D. Xu, N. L. Harrison, G. E. Homanics, D. L. Farber, C. W. Emala, GABA A receptor alpha4-subunit knockout en-

- hances lung inflammation and airway reactivity in a murine asthma model, *American Journal of Physiology - Lung Cellular and Molecular Physiology* 313 (2017) L406—L415.
- ⁷J. Egea, I. Buendia, E. Parada, E. Navarro, R. León, M. G. Lopez, Anti-inflammatory role of microglial alpha7 nAChRs and its role in neuroprotection, 2015.
- ⁸G. L. Cornelison, N. C. Pflanz, M. E. Tipps, S. J. Mihic, Identification and characterization of heptapeptide modulators of the glycine receptor, *European Journal of Pharmacology* 780 (2016) 252–259.
- ⁹W. Xiong, T. Cui, K. Cheng, F. Yang, S.-R. Chen, D. Willenbring, Y. Guan, H.-L. Pan, K. Ren, Y. Xu, L. Zhang, Cannabinoids suppress inflammatory and neuropathic pain by targeting alpha3 glycine receptors, *The Journal of Experimental Medicine* 209 (2012) 1121–1134.
- ¹⁰J. Walstab, G. Rappold, B. Niesler, 5-HT(3) receptors: role in disease and target of drugs, *Pharmacology & Therapeutics* 128 (2010) 146–169.
- ¹¹R. Picciotto, Marina, Neuroprotection via nAChRs: the role of nAChRs in neurodegenerative disorders such as Alzheimer's and Parkinson's disease, *Frontiers in Bioscience* 13 (2008) 492.
- ¹²C. M. Martin-Ruiz, J. A. Court, E. Molnar, M. Lee, C. Gotti, A. Mamalaki, T. Tsouloufis, S. Tzartos, C. Ballard, R. H. Perry, E. K. Perry, Alpha4 but not alpha3 and alpha7 nicotinic acetylcholine receptor subunits are lost from the temporal cortex in Alzheimer's disease, *Journal of Neurochemistry* 73 (1999) 1635–1640.
- ¹³A. S. Arnold, M. Gueye, S. Guettier-Sigrist, I. Courdier-Fruh, G. Coupin, P. Poindron, J. P. Gies, Reduced expression of nicotinic AChRs in myotubes from spinal muscular atrophy I patients, *Laboratory Investigation* 84 (2004) 1271–1278.
- ¹⁴S. N. Haydar, J. Dunlop, Neuronal nicotinic acetylcholine receptors - targets for the development of drugs to treat cognitive impairment associated with schizophrenia and alzheimer's disease., *Current topics in medicinal chemistry* 10 (2010) 144–152.
- ¹⁵V. A. Lennon, L. G. Ermilov, J. H. Szurszewski, S. Vernino, Immunization with neuronal nicotinic acetylcholine receptor induces neurological autoimmune disease, *Journal of Clinical Investigation* 111 (2003) 907–913.
- ¹⁶S. Kumari, V. Borroni, A. Chaudhry, B. Chanda, R. Massol, S. Mayor, F. J. Barrantes, Nicotinic acetylcholine receptor is internalized via a Rac-dependent, dynamin-independent endocytic pathway, *Journal of Cell Biology* 181 (2008) 1179–1193.
- ¹⁷J. E. Baenziger, J. A. Domville, J. P. D. Therien, The role of cholesterol in the activation of nicotinic acetylcholine receptors., *Current topics in membranes* 80 (2017) 95–137.

- ¹⁸A. W. Dalziel, E. S. Rollins, M. G. McNamee, The effect of cholesterol on agonist-induced flux in reconstituted acetylcholine receptor vesicles, *FEBS Letters* 122 (1980) 193–196.
- ¹⁹J. F. Ellena, M. A. Blazing, M. G. McNamee, Lipid-Protein Interactions in Reconstituted Membranes Containing Acetylcholine Receptor, *Biochemistry* 22 (1983) 5523–5535.
- ²⁰M. Criado, H. Eibl, F. J. Barrantes, Corrections: Effects of Lipids on Acetylcholine Receptor. Essential Need of Cholesterol for Maintenance of Agonist-Induced State Transitions in Lipid Vesicles: (*Biochemistry* (1982) 21(15) (3622–3629) (10.1021/bi00258a015)), *Biochemistry* 22 (1983) 524.
- ²¹T. M. Fong, M. G. McNamee, Correlation between acetylcholine receptor function and structural properties, *Biochemistry* 25 (1986) 830–840.
- ²²T. M. Fong, M. G. McNamee, Stabilization of Acetylcholine Receptor Secondary Structure by Cholesterol and Negatively Charged Phospholipids in Membranes, *Biochemistry* 26 (1987) 3871–3880.
- ²³O. T. Jones, M. G. McNamee, Annular and Nonannular Binding Sites for Cholesterol Associated with the Nicotinic Acetylcholine Receptor, *Biochemistry* 27 (1988) 2364–2374.
- ²⁴C. Sunshine, M. G. McNamee, Lipid modulation of nicotinic acetylcholine receptor function: the role of membrane lipid composition and fluidity, *Biochim Biophys Acta* 1191 (1994) 59–64.
- ²⁵C. J. DaCosta, S. A. Medaglia, N. Lavigne, S. Wang, C. L. Carswell, J. E. Baenzinger, Anionic lipids allosterically modulate multiple nicotinic acetylcholine receptor conformational equilibria, *Journal of Biological Chemistry* 284 (2009) 33841–33849.
- ²⁶S. B. Mantipragada, L. I. Horváth, H. R. Arias, G. Schwarzmann, K. Sandhoff, F. J. Barrantes, D. Marsh, Lipid-protein interactions and effect of local anesthetics in acetylcholine receptor-rich membranes from *Torpedo marmorata* electric organ, *Biochemistry* 42 (2003) 9167–9175.
- ²⁷F. J. Barrantes, Cholesterol effects on nicotinic acetylcholine receptor: Cellular aspects, *Subcellular Biochemistry* 51 (2010) 467–487.
- ²⁸C. J. Baier, J. Fantini, F. J. Barrantes, Disclosure of cholesterol recognition motifs in transmembrane domains of the human nicotinic acetylcholine receptor, *Scientific Reports* 1 (2011) 69.
- ²⁹Y. Zhou, M. E. Nelson, A. Kuryatov, C. Choi, J. Cooper, J. Lindstrom, Human $\alpha 4\beta 2$ acetylcholine receptors formed from linked subunits., *The Journal of neuroscience : the official journal of the Society for Neuroscience* 23 (2003) 9004–9015.

- ³⁰G. Gamba, W. G. Hill, N. M. Southern, B. Maciver, E. Potter, G. Apodaca, C. P. Smith, M. L. Zeidel, G. Warren, Isolation and characterization of the *Xenopus* oocyte plasma membrane : a new method for studying activity of water and solute transporters, *American Journal of Physiology-Renal Physiology* 15261 (2005) 217–224.
- ³¹Q. Chen, M. N. Kinde, P. Arjunan, M. M. Wells, A. E. Cohen, Y. Xu, P. Tang, Direct Pore Binding as a Mechanism for Isoflurane Inhibition of the Pentameric Ligand-gated Ion Channel ELIC, *Scientific Reports* 5 (2015) 13833.
- ³²N. Kouvatso, P. Giastas, D. Chroni-Tzartou, C. Pouloupoulou, S. J. Tzartos, Crystal structure of a human neuronal nAChR extracellular domain in pentameric assembly: Ligand-bound alpha2 homopentamer, *Proceedings of the National Academy of Sciences* 113 (2016) 9635–9640.
- ³³M. Nys, E. Wijckmans, A. Farinha, Ö. Yoluk, M. Andersson, M. Brams, R. Spurny, S. Peigneur, J. Tytgat, E. Lindahl, C. Ulens, Allosteric binding site in a Cys-loop receptor ligand-binding domain unveiled in the crystal structure of ELIC in complex with chlorpromazine, *Proceedings of the National Academy of Sciences* 113 (2016) E6696—E6703.
- ³⁴L. Polovinkin, G. Ghérici Hassaine, J. Perot, E. Neumann, A. A. Jensen, S. N. Lefebvre, P.-J. Corringer, J. Neyton, C. Chipot, F. Dehez, G. Schoehn, H. Nury, Conformational transitions of the serotonin 5-HT 3 receptor, *Nature* (2018).
- ³⁵S. X. Moffett, E. A. Klein, G. Brannigan, J. V. Martin, L-3,3',5-triiodothyronine and pregnenolone sulfate inhibit Torpedo nicotinic acetylcholine receptors, *PLoS ONE* 14 (2019) 1–18.
- ³⁶P. Kumar, Y. Wang, Z. Zhang, Z. Zhao, G. D. Cymes, E. Tajkhorshid, C. Grosman, Cryo-EM structures of a lipid-sensitive pentameric ligand-gated ion channel embedded in a phosphatidylcholine-only bilayer, *Proceedings of the National Academy of Sciences of the United States of America* 117 (2020) 1788–1798.
- ³⁷L. Conti, A. Limon, E. Palma, R. Miledi, Microtransplantation of cellular membranes from squid stellate ganglion reveals ionotropic GABA receptors, *Biological Bulletin* 224 (2013) 47–52.
- ³⁸C. Cotman, M. L. Blank, A. Moehl, F. Snyder, Lipid Composition of Synaptic Plasma Membranes Isolated from Rat Brain by Zonal Centrifugation, *Biochemistry* 8 (1969) 4606–4612.
- ³⁹R. Taguchi, M. Ishikawa, Precise and global identification of phospholipid molecular species by an Orbitrap mass spectrometer and automated search engine Lipid Search, *Journal of Chromatography A* (2010).

- ⁴⁰W. C. Breckenridge, I. G. Morgan, J. P. Zanetta, G. Vincendon, Adult rat brain synaptic vesicles II. Lipid composition, *BBA - General Subjects* 320 (1973) 681–686.
- ⁴¹H. I. Ingólfsson, T. S. Carpenter, H. Bhatia, P. T. Bremer, S. J. Marrink, F. C. Lightstone, Computational Lipidomics of the Neuronal Plasma Membrane, *Biophysical Journal* 113 (2017) 2271–2280.
- ⁴²T. G. McEvoy, G. D. Coull, P. J. Broadbent, J. S. M. Hutchinson, B. K. Speake, Fatty acid composition of lipids in immature cattle, pig and sheep oocytes with intact zona pellucida, *J Reprod Fertil* 118 (2000) 163–170.
- ⁴³J. Y. Kim, M. Kinoshita, M. Ohnishi, Y. Fukui, Lipid and fatty acid analysis of fresh and frozen-thawed immature and in vitro matured bovine oocytes, *Reproduction* 122 (2001) 131–138.
- ⁴⁴G. van Meer, A. I. P. M. de Kroon, Lipid map of the mammalian cell, *Journal of Cell Science* 124 (2010) 5–8.
- ⁴⁵J. H. Lorent, K. R. Levental, L. Ganesan, G. Rivera-Longsworth, E. Sezgin, M. Doktorova, E. Lyman, I. Levental, Plasma membranes are asymmetric in lipid unsaturation, packing and protein shape, *Nature Chemical Biology* 16 (2020) 644–652.
- ⁴⁶H. I. Ingólfsson, M. N. Melo, F. J. Van Eerden, C. Arnarez, C. A. Lopez, T. A. Wassenaar, X. Periole, A. H. De Vries, D. P. Tieleman, S. J. Marrink, Lipid organization of the plasma membrane, *Journal of the American Chemical Society* 136 (2014) 14554–14559.
- ⁴⁷F. J. Barrantes, The lipid environment of the nicotinic acetylcholine receptor in native and reconstituted membrane, *Critical Reviews in Biochemistry and Molecular Biology* 24 (1989) 437–478.
- ⁴⁸O. Quesada, C. González -Freire, M. C. Ferrer, J. O. Colón -Sáez, E. Fernández-García, J. Mercado, A. Dávila, R. Morales, J. A. Lasalde-Dominicci, Uncovering the lipidic basis for the preparation of functional nicotinic acetylcholine receptor detergent complexes for structural studies, *Scientific Reports* 6 (2016) 32766.
- ⁴⁹R. K. McNamara, M. Ostrander, W. Abplanalp, N. M. Richtand, S. C. Benoit, D. J. Clegg, Modulation of phosphoinositide-protein kinase C signal transduction by omega-3 fatty acids: Implications for the pathophysiology and treatment of recurrent neuropsychiatric illness, *Prostaglandins Leukotrienes and Essential Fatty Acids* 75 (2006) 237–257.
- ⁵⁰R. K. McNamara, R. Jandacek, T. Rider, P. Tso, K. E. Stanford, C. G. Hahn, N. M. Richtand, Deficits in docosahexaenoic acid and associated elevations in the metabolism of arachidonic acid and saturated fatty acids in the postmortem orbitofrontal cortex of patients with bipolar

- disorder, *Psychiatry Research* 160 (2008) 285–299.
- ⁵¹M. Maekawa, A. Watanabe, Y. Iwayama, T. Kimura, K. Hamazaki, S. Balan, H. Ohba, Y. Hisano, Y. Nozaki, T. Ohnishi, M. Toyoshima, C. Shimamoto, K. Iwamoto, M. Bundo, N. Osumi, E. Takahashi, A. Takashima, T. Yoshikawa, Polyunsaturated fatty acid deficiency during neurodevelopment in mice models the prodromal state of schizophrenia through epigenetic changes in nuclear receptor genes, *Translational Psychiatry* 7 (2017) 1–11.
- ⁵²R. M. Adibhatla, J. F. Hatcher, *Role of lipids in brain injury and diseases*, 2007.
- ⁵³M. Schneider, B. Levant, M. Reichel, E. Gulbins, J. Kornhuber, C. P. Müller, *Lipids in psychiatric disorders and preventive medicine*, 2017.
- ⁵⁴N. Koga, J. Ogura, F. Yoshida, K. Hattori, H. Hori, E. Aizawa, I. Ishida, H. Kunugi, Altered polyunsaturated fatty acid levels in relation to proinflammatory cytokines, fatty acid desaturase genotype, and diet in bipolar disorder, *Translational Psychiatry* 9 (2019).
- ⁵⁵K. Hamazaki, M. Maekawa, T. Toyota, B. Dean, T. Hamazaki, T. Yoshikawa, Fatty acid composition of the postmortem prefrontal cortex of patients with schizophrenia, bipolar disorder, and major depressive disorder, *Psychiatry Research* 227 (2015) 353–359.
- ⁵⁶M. Peet, Eicosapentaenoic acid in the treatment of schizophrenia and depression: Rationale and preliminary double-blind clinical trial results, *Prostaglandins Leukotrienes and Essential Fatty Acids* 69 (2003) 477–485.
- ⁵⁷C. Bushe, C. Paton, The potential impact of antipsychotics on lipids in schizophrenia: Is there enough evidence to confirm a link?, *Journal of Psychopharmacology* 19 (2005) 76–83.
- ⁵⁸G. E. Berger, S. Smesny, G. P. Amminger, Bioactive lipids in schizophrenia, *International Review of Psychiatry* 18 (2006) 85–98.
- ⁵⁹J. A. Conquer, M. C. Tierney, J. Zecevic, W. J. Bettger, R. H. Fisher, Fatty acid analysis of blood plasma of patients with alzheimer's disease, other types of dementia, and cognitive impairment, *Lipids* 35 (2000) 1305–1312.
- ⁶⁰G. Di Paolo, T.-W. Kim, Linking lipids to Alzheimer's disease: cholesterol and beyond, *Nature Reviews Neuroscience* 12 (2011) 284–296.
- ⁶¹S. A. L. Bennett, N. Valenzuela, H. Xu, B. Franko, S. Fai, D. Figeys, Using neurolipidomics to identify phospholipid mediators of synaptic (dys)function in Alzheimer's Disease, *Frontiers in Physiology* 4 JUL (2013) 1–16.
- ⁶²R. S. Yadav, N. K. Tiwari, *Lipid Integration in Neurodegeneration: An Overview of Alzheimer's Disease*, 2014.

- ⁶³P. V. Escribá, Membrane-lipid therapy: A historical perspective of membrane-targeted therapies — From lipid bilayer structure to the pathophysiological regulation of cells, *Biochimica et Biophysica Acta - Biomembranes* 1859 (2017) 1493–1506.
- ⁶⁴G. H. Addona, H. Sandermann, M. A. Kloczewiak, S. S. Husain, K. W. Miller, Where does cholesterol act during activation of the nicotinic acetylcholine receptor?, *Biochimica et Biophysica Acta - Biomembranes* 1370 (1998) 299–309.
- ⁶⁵D. Lavery, P. Thomas, M. Field, O. J. Andersen, M. G. Gold, P. C. Biggin, M. Gielen, T. G. Smart, Crystal structures of a GABA A -receptor chimera reveal new endogenous neurosteroid-binding sites, *Nature Structural and Molecular Biology* 24 (2017) 977–985.
- ⁶⁶M. M. Budelier, W. W. L. Cheng, Z. W. Chen, J. R. Bracamontes, Y. Sugawara, K. Krishnan, L. Mydock-McGrane, D. F. Covey, A. S. Evers, Common binding sites for cholesterol and neurosteroids on a pentameric ligand-gated ion channel, *Biochimica et Biophysica Acta - Molecular and Cell Biology of Lipids* 1864 (2019) 128–136.
- ⁶⁷S. Basak, N. Schmandt, Y. Gicheru, S. Chakrapani, Crystal structure and dynamics of a lipid-induced potential desensitized-state of a pentameric ligand-gated channel, *eLife* 6 (2017) e23886.
- ⁶⁸C. M. Hénault, C. Govaerts, R. Spurny, M. Brams, A. Estrada-Mondragon, J. Lynch, D. Bertrand, E. Pardon, G. L. Evans, K. Woods, B. W. Elberson, L. G. Cuello, G. Brannigan, H. Nury, J. Steyaert, J. E. Baenziger, C. Ulens, A lipid site shapes the agonist response of a pentameric ligand-gated ion channel, *Nature Chemical Biology* (2019).
- ⁶⁹J. J. Kim, A. Gharpure, J. Teng, Y. Zhuang, R. J. Howard, S. Zhu, C. M. Noviello, R. M. Walsh, E. Lindahl, R. E. Hibbs, Shared structural mechanisms of general anaesthetics and benzodiazepines, *Nature* 585 (2020) 303–308.
- ⁷⁰A. Tong, F. F. Hsu, P. A. Schmidpeter, C. M. Nimigeon, L. Sharp, G. Brannigan, W. W. Cheng, Direct binding of phosphatidylglycerol at specific sites modulates desensitization of a Ligand-gated ion channel, *eLife* 8 (2019).
- ⁷¹G. Brannigan, J. Henin, R. Law, R. Eckenhoff, M. L. Klein, Embedded cholesterol in the nicotinic acetylcholine receptor, *Proceedings of the National Academy of Sciences* 105 (2008) 14418–14423.
- ⁷²J. Hénin, R. Salari, S. Murlidaran, G. Brannigan, A predicted binding site for cholesterol on the GABAA receptor, *Biophysical Journal* 106 (2014) 1938–1949.

- ⁷³J. Domański, S. J. Marrink, L. V. Schäfer, Transmembrane helices can induce domain formation in crowded model membranes, *Biochimica et Biophysica Acta - Biomembranes* 1818 (2012) 984–994.
- ⁷⁴M. Chavent, A. L. Duncan, M. S. Sansom, Molecular dynamics simulations of membrane proteins and their interactions: from nanoscale to mesoscale This review comes from a themed issue on Biophysical and molecular biological methods, *Current Opinion in Structural Biology* 40 (2016) 8–16.
- ⁷⁵T. S. Carpenter, C. A. López, C. Neale, C. Montour, H. I. Ingólfsson, F. Di Natale, F. C. Lightstone, S. Gnanakaran, Capturing Phase Behavior of Ternary Lipid Mixtures with a Refined Martini Coarse-Grained Force Field, *Journal of Chemical Theory and Computation* 14 (2018) 6050–6062.
- ⁷⁶H. I. Ingólfsson, H. Bhatia, T. Zeppelin, W. F. Bennett, K. A. Carpenter, P. C. Hsu, G. Dharaman, P. T. Bremer, B. Schiøtt, F. C. Lightstone, T. S. Carpenter, Capturing Biologically Complex Tissue-Specific Membranes at Different Levels of Compositional Complexity, *The journal of physical chemistry. B* 124 (2020) 7819–7829.
- ⁷⁷T. T. Joseph, J. S. Mincer, Common internal allosteric network links anesthetic binding sites in a pentameric ligand-gated ion channel, *PLoS ONE* 11 (2016) 1–20.
- ⁷⁸L. Sharp, R. Salari, G. Brannigan, Boundary lipids of the nicotinic acetylcholine receptor: Spontaneous partitioning via coarse-grained molecular dynamics simulation, *Biochimica et Biophysica Acta - Biomembranes* 1861 (2019) 887–896.
- ⁷⁹K. Woods, L. Sharp, G. Brannigan, Untangling Direct and Domain-Mediated Interactions Between Nicotinic Acetylcholine Receptors in DHA-Rich Membranes, *Journal of Membrane Biology* 252 (2019) 385–396.
- ⁸⁰S. J. Marrink, V. Corradi, P. C. Souza, H. I. Ingólfsson, D. P. Tieleman, M. S. Sansom, Computational Modeling of Realistic Cell Membranes, *Chemical Reviews* 119 (2019) 6184–6226.
- ⁸¹K. A. Wilson, H. I. MacDermott-Opeskin, E. Riley, Y. Lin, M. L. O’Mara, Understanding the Link between Lipid Diversity and the Biophysical Properties of the Neuronal Plasma Membrane, *Biochemistry* 59 (2020) 3010–3018.
- ⁸²J. Lorent, L. Ganesan, G. Rivera-Longsworth, E. Sezgin, K. Levental, E. Lyman, I. Levental, The Molecular and Structural Asymmetry of the Plasma Membrane, *bioRxiv* (2019) 698837.
- ⁸³N. Unwin, Refined structure of the nicotinic acetylcholine receptor at 4 Å resolution, *Journal of Molecular Biology* 346 (2005) 967–989.

- ⁸⁴D. H. de Jong, G. Singh, W. F. D. Bennett, C. Arnarez, T. A. Wassenaar, L. V. Schäfer, X. Periole, D. P. Tieleman, S. J. Marrink, Improved parameters for the martini coarse-grained protein force field., *Journal of chemical theory and computation* 9 (2013) 687–697.
- ⁸⁵T. A. Wassenaar, H. I. Ingólfsson, R. A. Böckmann, D. P. Tieleman, S. J. Marrink, Computational lipidomics with insane: A versatile tool for generating custom membranes for molecular simulations, *Journal of Chemical Theory and Computation* 11 (2015) 2144–2155.
- ⁸⁶H. J. Berendsen, D. van der Spoel, R. van Drunen, GROMACS: A message-passing parallel molecular dynamics implementation, *Computer Physics Communications* 91 (1995) 43–56.
- ⁸⁷M. J. Abraham, T. Murtola, R. Schulz, S. Páll, J. C. Smith, B. Hess, E. Lindah, Gromacs: High performance molecular simulations through multi-level parallelism from laptops to supercomputers, *SoftwareX* 1-2 (2015) 19–25.
- ⁸⁸X. Periole, M. Cavalli, S. J. Marrink, M. A. Ceruso, Combining an elastic network with a coarse-grained molecular force field: Structure, dynamics, and intermolecular recognition, *Journal of Chemical Theory and Computation* 5 (2009) 2531–2543.
- ⁸⁹G. B. Liam Sharp, Densitymap, github, 2020.
- ⁹⁰G. Brannigan, F. L. Brown, Contributions of Gaussian curvature and nonconstant lipid volume to protein deformation of lipid bilayers, *Biophysical Journal* 92 (2007) 864–876.
- ⁹¹K. S. Kim, J. Neu, G. Oster, Curvature-mediated interactions between membrane proteins, *Biophysical Journal* 75 (1998) 2274–2291.
- ⁹²N. Dan, P. Pincus, S. A. Safran, Membrane-Induced Interactions between Inclusions, *Langmuir* 9 (1993) 2768–2771.
- ⁹³M. Goulian, Inclusions in membranes, *Current Opinion in Colloid and Interface Science* 1 (1996) 358–361.
- ⁹⁴M. Goulian, R. Bruinsma, P. Pincus, Long-range forces in heterogeneous fluid membranes, *Epl* 23 (1993) 125–128.
- ⁹⁵J. B. Fournier, P. Galatola, High-order power series expansion of the elastic interaction between conical membrane inclusions, *European Physical Journal E* 38 (2015) 1–8.
- ⁹⁶R. Salari, T. Joseph, R. Lohia, J. Henin, G. Brannigan, A streamlined, general approach for computing ligand binding free energies and its application to GPCR-bound cholesterol, *Journal of Chemical Theory and Computation* (2018).
- ⁹⁷J. E. Baenziger, M.-I. Morris, T. E. Darsaut, S. E. Ryan, Effect of Membrane Lipid Composition on the Conformational Equilibria of the Nicotinic Acetylcholine Receptor*, *Journal of*

Biological Chemistry 275 (2000) 777–784.

- ⁹⁸J. J. Wenz, F. J. Barrantes, Nicotinic acetylcholine receptor induces lateral segregation of phosphatidic acid and phosphatidylcholine in reconstituted membranes, *Biochemistry* 44 (2005) 398–410.
- ⁹⁹A. K. Hamouda, M. Sanghvi, D. Sauls, T. K. Machu, M. P. Blanton, Assessing the lipid requirements of the *Torpedo californica* nicotinic acetylcholine receptor, *Biochemistry* 45 (2006) 4327–4337.
- ¹⁰⁰M. J. Thompson, J. E. Baenziger, Structural basis for the modulation of pentameric ligand-gated ion channel function by lipids, *Biochimica et Biophysica Acta (BBA) - Biomembranes* 1862 (2020) 183304.